International Journal of Solids and Structures 51 (2014) 144–153

Contents lists available at ScienceDirect

International Journal of Solids and Structures

journal homepage: www.elsevier.com/locate/ijsolstr

Computational analysis of liquid crystalline elastomer membranes: Changing Gaussian curvature without stretch energy

F. Cirak [a,*], Q. Long [a,1], K. Bhattacharya [b], M. Warner [c]

[a] Department of Engineering, University of Cambridge, Cambridge CB2 1PZ, UK
[b] Division of Engineering and Applied Science, California Institute of Technology, Pasadena, CA 91125, USA
[c] Cavendish Laboratory, University of Cambridge, Cambridge CB3 0HE, UK

ARTICLE INFO

Article history:
Received 17 December 2012
Received in revised form 16 August 2013
Available online 8 October 2013

Keywords:
Liquid crystalline elastomer
Nematic elastomer
Soft material
Non-developable surface
Finite elements

ABSTRACT

Liquid crystalline elastomers (LCEs) can undergo extremely large reversible shape changes when exposed to external stimuli, such as mechanical deformations, heating or illumination. The deformation of LCEs result from a combination of directional reorientation of the nematic director and entropic elasticity. In this paper, we study the energetics of initially flat, thin LCE membranes by stress driven reorientation of the nematic director. The energy functional used in the variational formulation includes contributions depending on the deformation gradient and the second gradient of the deformation. The deformation gradient models the in-plane stretching of the membrane. The second gradient regularises the non-convex membrane energy functional so that infinitely fine in-plane microstructures and infinitely fine out-of-plane membrane wrinkling are penalised. For a specific example, our computational results show that a non-developable surface can be generated from an initially flat sheet at cost of only energy terms resulting from the second gradients. That is, Gaussian curvature can be generated in LCE membranes without the cost of stretch energy in contrast to conventional materials.

1. Introduction

1.1. Liquid crystalline elastomers (LCEs)

Elastomers are the base constituent of LCEs and are composed of long, flexible molecular chains which are sufficiently linked to each other by permanent chemical bonds (crosslinks) so that they form a solid. Such rubbery solids are soft in the sense that their shear moduli are of the order of 10^{-4} times their compression moduli, that is they essentially deform at constant volume. Such disparity in moduli arises because there are few crosslinks and the long chains between them are free to move as in their liquid state and in particular can extend enormously from their random coil conformations before their finite molecular length is sensed in any way. This freedom means that elastomers are capable of large macroscopic extensions. By contrast, liquid crystals are true liquids that are not just fluid-like at the molecular scale (as elastomers are) but which can flow. They have no long range positional order, but their constituent molecular rods are orientationally ordered about a direction called the director $\boldsymbol{n}$, a unit vector.[2]

Elastomers and liquid crystals can be combined by chemically bonding rods to flexible polymer chains so that the chains remain fluid-like but are anisotropic in shape to an extent depending on the degree of rod alignment with $\boldsymbol{n}$. When such long chains are loosely crosslinked to form elastomers both the local fluidity of elastomers and the orientational order of liquid crystals and their consequent properties of soft extensibility and of anisotropy persist, including the freedom to rotate the director to new directions. However, entirely new properties also emerge in these LCEs. Their unique properties arise from the rod orientation changing the chain shapes and when the chains are crosslinked, changes in the degree of order being reflected in changes of shape of the bulk material. They can deform dramatically under heat, reversibly changing their lengths by many times their original length. When the temperature is high enough, the distribution of molecular directions is random and the material is in an isotropic liquid phase. This phase is called the *isotropic phase*. On the other hand, when the temperature is lower than the critical value, molecules

* Corresponding author. Tel.: +44 1223 332716; fax: +44 1223 339713.
E-mail addresses: f.cirak@eng.cam.ac.uk (F. Cirak), quan@ices.utexas.edu (Q. Long), bhatta@caltech.edu (K. Bhattacharya), mw141@cam.ac.uk (M. Warner).

[1] This author is currently a joint postdoctoral scholar at UT Austin and KAUST.

[2] Actually this vector has only its ends identified since nematic order is quadrupolar and does not distinguish between $+\boldsymbol{n}$ and $-\boldsymbol{n}$. Thus $\boldsymbol{n}$ lives on the unit sphere with identified poles, which is isomorphic to the projective plane. This property of $\boldsymbol{n}$ requires energy expressions to have terms with an even number of powers of $\boldsymbol{n}$.

0020-7683/$ - see front matter © 2013 Elsevier Ltd. All rights reserved.
http://dx.doi.org/10.1016/j.ijsolstr.2013.09.019

become locally aligned about the director and start to couple with macroscopic deformations of the material matrix. This phase is called the *nematic phase*. Order can also be changed by light in many elastomers where the rods are dye molecules and thus light (including its polarisation) offers subtle control of mechanics. Recently these properties have been explored in many applications, e.g. artificial muscles and smart actuators (Bhattacharya et al., 2001; van Oosten et al., 2008; Corbett and Warner, 2009).

A further remarkable phenomenon in LCEs is the accommodating of externally prescribed shape changes by re-orienting the director, that is the direction of order, and hence the direction of natural elongation of the body. When these redirected elongations correspond exactly to the imposed distortions of the body, they allow deformation to occur at no or low energy cost — nematic soft elasticity (Warner and Terentjev, 2007). See Fig. 1 for a schematic illustration of this accommodation at no energy cost. The ellipsoid in the figure characterises the chain shape distribution and the box indicates the shape of an initially square specimen. Sometimes these soft deformations have to be realised via laminates of alternating soft deformations as shown in Fig. 2. Lamination allows elongation softly in the presence of boundaries, clamps and other possible constraints that are incompatible, for instance, with any gross shear, as in Fig. 1(b). This possibility was initially envisaged by Verwey et al. (1996) and observed by Finkelmann et al. (1997) for simple strips clamped at their ends and stretched perpendicular to an initial transverse director. Stripes of alternating direction of director rotation and with simple shear occur. Laminates can add then their effect together to overall closely obey boundary conditions. Because regions individually suffer soft deformation, together they achieve the imposed macroscopic deformation while only costing the very soft elastic penalty associated with the deformations as in Fig. 1. When the macroscopic deformation exceeds that which can be achieved by realigning the director in the stretching direction and accommodating stretch by directing the naturally extended direction of the body along it, the nematic elastomer deforms with the usual energy cost of a normal rubber. DeSimone and Dolzmann (2002) have characterised the overall macroscopic behaviour after the material forms microstructure (or the quasiconvex envelope), including all possible macroscopic soft deformations.

1.2. Liquid crystalline glasses

Closely related to LCEs are liquid crystal glasses. These are also liquid crystalline solids, but with a high cross-link density to be glassy. They undergo isotropic to nematic transitions as LCEs. However, unlike LCEs, the director can not reorient itself relative to the polymer background and thus do not display soft behaviour. van Oosten et al. (2008, 2009) have used liquid crystal glasses to make highly efficient microscale actuators. The idea is to use pre-coded non-uniform director fields, or non-uniformly absorbed external stimuli through the thickness of a solid with a uniform director. These have been analysed in some detail in Warner and Mahadevan (2004), Warner et al. (2010a,b).

In an alternate approach, Modes et al. (2011) demonstrated that initially flat membranes of liquid crystal glass with director oriented uniformly through the thickness but containing a topological defect can deform into shapes with non-zero Gaussian curvature without any cost of stretching. Since the deformation is uniform through the thickness, the energy and force available for actuation through these modes would be proportional to thickness and thus higher than in bending based actuators.

1.3. Aims and approach

The aims of this paper are two fold. First, we show that the soft deformation of LCEs can be exploited to create Gaussian curvature change with very little energy. Specifically, we show that an initially flat membrane of LCE can be deformed into the shape of a non-developable surface with no stretch energy. This is in remarkable contrast with ordinary elastic membranes that resist any change of Gaussian curvature and thus require significant elastic energy to be deformed into a non-developable shape. Indeed this resistance is so strong that it gives rise to wrinkling and other instabilities. The fact that LCE membranes can change Gaussian curvature freely points to its potential application as deformable skins. Further, it also points to its use as actuators: by inducing the isotropic to nematic transition by light or heat one can transform a membrane between a flexible state (nematic) and a stiff flat state (isotropic). Such an actuator would again possess high energy and force proportional to thickness. Second, we develop a numerical method to study large deformations of these nonlinear materials. This requires the careful treatment of higher gradients, geometric nonlinearity and material non-convexity.

To these ends, we consider the Verwey–Warner–Terentjev (VWT) nematic elastic energy (Verwey et al., 1996) in the form introduced by DeSimone and Dolzmann (2002). We show that this energy can also be phenomenologically motivated by assuming a multiplicative decomposition of the deformation gradient into an elastic component and a component representing the reorientation of the nematic director. Subsequently, we use the fact that the lateral extent of the membrane is much larger than its thickness and follow Le Dret and Raoult (1995) and Bhattacharya and James (1999) to derive a model for thin membranes. The derived membrane energy functional has two parts. The first part takes account of in-plane stretching and depends on the first gradient of the deformation. The second part is a regularisation term and depends on the Laplacian, i.e. second gradient, of the deformation (Dondl et al., 2007; Kohn and Müller, 1992). The membrane energy functional is discretised with the finite element method using box-spline basis functions. The same numerical technique had previously been applied to thin shells Cirak et al., 2000; Cirak and

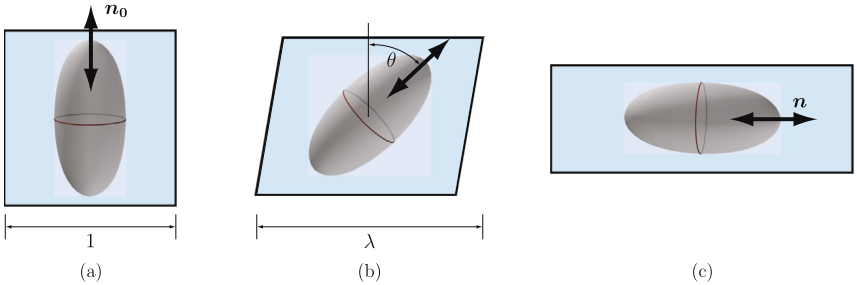

Fig. 1. An elongation imposed perpendicular to the initial director $\boldsymbol{n}_0$ (a) causes it and its associated anisotropic distribution of chain shapes (the ellipsoid) to rotate (c). The natural shape of the body thereby changes, with a suitable component of elongation along the imposed direction, but also with concomitant sympathetic shears (b). Since the natural chain shapes are not distorted, but only rotated, there is no elastic cost of such shape change ("soft elasticity"). When rotation is complete, shear ceases and further imposed elongation can now no longer be accommodated by reorientation. The energy cost then rises to that of conventional rubber elasticity.

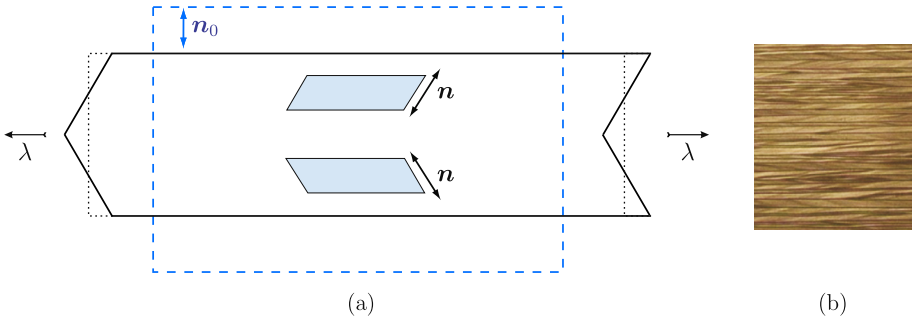

Fig. 2. Microstructure in a strip being extended from its initial configuration (dashed line) with director $\boldsymbol{n}_0$ (a). Two soft stripes of alternating shear (symbolically represented by the parallelograms) with director $\boldsymbol{n}$ add to give extension and decreased macroscopic shear. Experimentally, very fine stripes develop to accommodate the regions where shear is forbidden (b), image courtesy of Finkelmann et al. (1997).

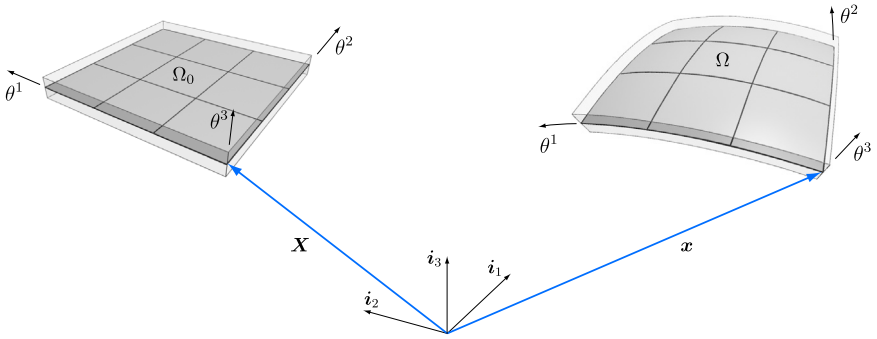

Fig. 3. The membrane in its reference and deformed configurations. The two coordinate vectors, $\boldsymbol{X}$ and $\boldsymbol{x}$, indicate the position of the same material point in the two configurations.

Ortiz, 2001; Cirak et al., 2003; Cirak and Long, 2011. Informally, box splines are the generalisation of b-splines to multi-dimensional domains.

The paper is organised as follows. In Section 2 we introduce the governing equation of the thin membrane. Specifically, we discuss in Section 2.1 the kinematic description of a surface undergoing finite deformations. Subsequently, in Section 2.2 the derivation of the LCE constitutive models with unconstrained and frozen director are introduced. The membrane energy functional, which serves as the starting point for the discretization, is introduced in Section 2.3. Its finite element discretization and the implemented numerical solution approach are discussed in Section 3. In Section 4 the developed numerical scheme is used to compute the deformation of a rectangular shaped initially flat membrane due to prescribed boundary displacements. In particular, the internal energy requirements of the different configurations of the LCEs are compared.

2. Governing equation of thin membranes

In this section, we first briefly review the kinematic description of the membrane and then introduce the constitutive model used for the liquid crystalline elastomer membrane.

2.1. Kinematic description

The membrane occupies in its reference configuration the domain $\Omega_0 = \omega_0 \times (-\frac{t}{2}, \frac{t}{2})$ with the mid-surface $\omega_0 \subset \mathbb{R}^2$ and the thickness t, see Fig. 3. The loaded membrane occupies after the deformation the domain $\Omega \subset \mathbb{R}^3$ with the mid-surface ω. As common, we parameterise the membrane with convective (curvilinear) coordinates so that a material point has throughout the deformation history the same coordinates $(\theta^1, \theta^2, \theta^3)$, see also (Cirak et al., 2000; Cirak and Ortiz, 2001). We take advantage of the geometry of Ω_0 and assume that (θ^1, θ^2) parameterise the mid-surface ω_0 while θ^3 parameterises the thickness.

The position vectors of the material points in the reference and deformed configurations are denoted with $\boldsymbol{X} = \boldsymbol{X}(\theta^1, \theta^2, \theta^3)$ and $\boldsymbol{x} = \boldsymbol{x}(\theta^1, \theta^2, \theta^3)$, respectively. The covariant basis vectors of the tangent space to the membrane surface are defined with[3]

$$\boldsymbol{A}_i = \frac{\partial \boldsymbol{X}}{\partial \theta^i}, \qquad \boldsymbol{a}_i = \frac{\partial \boldsymbol{x}}{\partial \theta^i}. \tag{1}$$

The corresponding contravariant basis vectors $\boldsymbol{A}^i$ and $\boldsymbol{a}^i$ follow from the relations

$$\boldsymbol{A}^i \cdot \boldsymbol{A}_j = \delta^i_j, \qquad \boldsymbol{a}^i \cdot \boldsymbol{a}_j = \delta^i_j, \tag{2}$$

where δ^i_j is the Kronecker delta.

Assuming the mapping from the reference to the deformed configuration is sufficiently smooth we can compute a deformation gradient

$$\boldsymbol{F} = \frac{\partial \boldsymbol{x}}{\partial \boldsymbol{X}} = \frac{\partial \boldsymbol{x}}{\partial \theta^i} \otimes \frac{\partial \theta^i}{\partial \boldsymbol{X}} = \boldsymbol{a}_i \otimes \boldsymbol{A}^i \qquad \left(\text{or}, x_{i,j} = \frac{\partial x_i}{\partial \theta^k} \frac{\partial \theta^k}{\partial X_j} \right). \tag{3}$$

The right Cauchy–Green strain tensor is defined as

$$\boldsymbol{C} = \boldsymbol{F}^{\mathsf{T}} \boldsymbol{F} = \boldsymbol{a}_i \cdot \boldsymbol{a}_j \boldsymbol{A}^i \otimes \boldsymbol{A}^j = a_{ij} \boldsymbol{A}^i \otimes \boldsymbol{A}^j, \tag{4}$$

where the three-by-three covariant metric tensor a_{ij} in the deformed configuration is the scalar product of the basis vectors. The left Cauchy–Green strain tensor is defined as

$$\boldsymbol{b} = \boldsymbol{F}\boldsymbol{F}^{\mathsf{T}} = \boldsymbol{A}^i \cdot \boldsymbol{A}^j \boldsymbol{a}_i \otimes \boldsymbol{a}_j = A^{ij} \boldsymbol{a}_i \otimes \boldsymbol{a}_j. \tag{5}$$

[3] Notation: The Greek indices take values one and two while the Latin indices take values one, two and three. Further, summation over repeated indices applies.

Here the scalar product of the basis vectors A^{ij} is the contravariant metric tensor in the reference configuration. For future use, we introduce the spectral representations of the Cauchy–Green tensors

$$\boldsymbol{C} = \sum_{i=1}^{3} (\lambda_i)^2 \, \boldsymbol{E}_i \otimes \boldsymbol{E}_i, \tag{6a}$$

$$\boldsymbol{b} = \sum_{i=1}^{3} (\lambda_i)^2 \, \boldsymbol{e}_i \otimes \boldsymbol{e}_i, \tag{6b}$$

where $\boldsymbol{E}_i$ and $\boldsymbol{e}_i$ are the eigenvectors and $\lambda_1 \geqslant \lambda_2 \geqslant \lambda_3$ are the principal values of $\boldsymbol{F}$.

We are interested in the deformation of thin membranes, and we shall thus be interested in the deformation of the mid-surface $\omega \times \{0\}$. This deformation is described as the mapping $\boldsymbol{X}(\theta^1, \theta^2, 0) \rightarrow \boldsymbol{x}(\theta^1, \theta^2, 0)$ and we may define the tangential deformation gradient as

$$\bar{\boldsymbol{F}} = \boldsymbol{a}_\alpha \otimes \boldsymbol{A}^\alpha \qquad \left(\text{or, } x_{i,j} = \frac{\partial x_i}{\partial \theta^\alpha} \frac{\partial \theta^\alpha}{\partial X_j} \right). \tag{7}$$

Comparing with (3), we see that $\boldsymbol{F} = \bar{\boldsymbol{F}} + \boldsymbol{a}_3 \otimes \boldsymbol{A}^3$. We define the tangential Cauchy–Green strain tensors to be

$$\bar{\boldsymbol{C}} = \bar{\boldsymbol{F}}^{\mathrm{T}} \bar{\boldsymbol{F}} = \sum_{\alpha=1}^{2} (\bar{\lambda}_\alpha)^2 \, \bar{\boldsymbol{E}}_\alpha \otimes \bar{\boldsymbol{E}}_\alpha, \tag{8a}$$

$$\bar{\boldsymbol{b}} = \bar{\boldsymbol{F}} \bar{\boldsymbol{F}}^{\mathrm{T}} = \sum_{\alpha=1}^{2} (\bar{\lambda}_\alpha)^2 \, \bar{\boldsymbol{e}}_\alpha \otimes \bar{\boldsymbol{e}}_\alpha, \tag{8b}$$

where $\bar{\lambda}_\alpha$ are the principal values of $\bar{\boldsymbol{F}}$. Note that in general the eigenvectors $\bar{\boldsymbol{E}}_\alpha$ may not coincide with the eigenvectors $\boldsymbol{E}_i$ and the principal values of $\bar{\boldsymbol{F}}$ may differ from those of $\boldsymbol{F}$.

2.2. Constitutive model

As discussed in the Introduction, liquid crystalline elastomer solids undergo a phase transformation at a critical temperature. Below the critical temperature, in the nematic phase the liquid crystalline mesogens order locally along the nematic director $\boldsymbol{n}$. The ordering takes place on a scale of nanometers, and we thus regard $\boldsymbol{n}$ as a continuum field. In ideal LCEs, the director can rotate freely (since the high temperature phase is isotropic). However, as a result of imperfections or non-idealities, the director has a preferred direction $\boldsymbol{n}_0$ (which may vary spatially). In a liquid crystalline glass, the director is frozen (i.e., unable to rotate freely). In the following, we begin with Verwey, Warner and Terentjev (VWT) (Verwey et al., 1996) model for ideal liquid crystal elastomers in a form given in DeSimone and Teresi (2009). We then modify it for non-ideal elastomers and glasses.

2.2.1. Unconstrained nematic director

We take the isotropic, high temperature state of the nematic as the reference configuration. The energy density of an *ideal* nematic elastomer with the isochoric deformation gradient $\boldsymbol{F}$ satisfying $\det \boldsymbol{F} = 1$ and nematic director $\boldsymbol{n}$ satisfying $|\boldsymbol{n}| = 1$ is given by

$$f(\boldsymbol{F}, \boldsymbol{n}) = \frac{\mu}{2} \mathrm{Tr} \, \left(\boldsymbol{F}^{\mathrm{T}} \boldsymbol{g}^{-2} \boldsymbol{F} \right), \tag{9}$$

where

$$\boldsymbol{g} = a^{-1/6} (\boldsymbol{I} + (a^{1/2} - 1) \boldsymbol{n} \otimes \boldsymbol{n}) \tag{10}$$

and μ is the shear modulus. The isochoric tensor $\boldsymbol{g}$ with $\det \boldsymbol{g} = 1$ is the spontaneous deformation of the elastomer determined by a material parameter $a > 1$.[4] It is easily verified that (9) is frame-indifferent and isotropic by recognising that $\boldsymbol{n}$ is an observable (hence spatial) quantity.

As an aside, since $\boldsymbol{g}$ is the spontaneous deformation, we can define $\boldsymbol{F}^e = \boldsymbol{g}^{-1} \boldsymbol{F}$ to be the elastic deformation of the polymer network. Then, we observe

$$f(\boldsymbol{F}, \boldsymbol{n}) = \frac{\mu}{2} \mathrm{Tr} \left((\boldsymbol{g}^{-1} \boldsymbol{F})^{\mathrm{T}} (\boldsymbol{g}^{-1} \boldsymbol{F}) \right) = \frac{\mu}{2} \mathrm{Tr} \left(\boldsymbol{F}^{e\mathrm{T}} \boldsymbol{F}^e \right). \tag{11}$$

Indeed the last expression is the most basic, isotropic, Neo-Hookean energy for cross-linked polymers. The decomposition $\boldsymbol{F}^e = \boldsymbol{g}^{-1} \boldsymbol{F}$ is similar to the multiplicative decomposition of the deformation gradient common, among others, in elastoplasticity and membrane wrinkling, see e.g. (Gurtin et al., 2010; Pipkin, 1994; Mosler and Cirak, 2009).

It is convenient to substitute (10) into (9) and rewrite it as

$$\begin{aligned} f(\boldsymbol{F}, \boldsymbol{n}) &= \frac{\mu a^{1/3}}{2} \left(\mathrm{Tr} \left(\boldsymbol{F}^{\mathrm{T}} \boldsymbol{F} \right) - (1 - a^{-1}) \boldsymbol{n} \cdot \boldsymbol{F} \boldsymbol{F}^{\mathrm{T}} \boldsymbol{n} \right) \\ &= \frac{\mu a^{1/3}}{2} \left(\mathrm{Tr} \left(\boldsymbol{C} \right) - (1 - a^{-1}) \boldsymbol{n} \cdot \boldsymbol{b} \boldsymbol{n} \right). \end{aligned} \tag{12}$$

In an *non-ideal* nematic elastomer, there is a preferred directional orientation $\boldsymbol{n}_0$ and the material becomes anisotropic. To reflect this, we follow Conti et al. (2002) (also Biggins et al., 2008) and modify the energy density to be

$$f(\boldsymbol{F}, \boldsymbol{n}) = \frac{\mu a^{1/3}}{2} \left(\mathrm{Tr} \boldsymbol{C} - (1 - a^{-1}) \boldsymbol{n} \cdot \boldsymbol{b} \boldsymbol{n} - \beta \boldsymbol{n}_0 \cdot \boldsymbol{C} \boldsymbol{n}_0 \right), \tag{13}$$

where we introduce the non-ideality parameter β. This can be expressed with principal stretches by recalling the spectral representation (6),

$$f(\boldsymbol{F}, \boldsymbol{n}) = \frac{\mu}{2 a^{1/3}} \left(\lambda_1^2 + \lambda_2^2 + \lambda_3^2 - (1 - a^{-1}) \sum_{i=1}^{3} \lambda_i^2 (\boldsymbol{e}_i \cdot \boldsymbol{n})^2 - \beta \sum_{i=1}^{3} \lambda_i^2 (\boldsymbol{E}_i \cdot \boldsymbol{n}_0)^2 \right) \tag{14}$$

subject to the incompressibility constraint $\lambda_1 \lambda_2 \lambda_3 = 1$.

Since the director is allowed to rotate, we obtain the mechanical energy density of the material to be

$$W(\boldsymbol{F}) = \min_{\boldsymbol{n}} f(\boldsymbol{F}, \boldsymbol{n}). \tag{15}$$

Now, since $a > 1$ and $0 < (1 - a^{-1}) \leqslant 1$ it is clear from (14) that the minimum value is attained at $\boldsymbol{n} = \boldsymbol{e}_1$. Therefore,

$$W(\boldsymbol{F}) = \frac{\mu a^{1/3}}{2} \left(\frac{\lambda_1^2}{a} + \lambda_2^2 + \lambda_3^2 - \beta \sum_{i=1}^{3} \lambda_i^2 (\boldsymbol{E}_i \cdot \boldsymbol{n}_0)^2 \right), \tag{16}$$

again subject to the incompressibility constraint $\lambda_1 \lambda_2 \lambda_3 = 1$.

2.2.2. Frozen nematic director

In LCEs with a so-called frozen nematic director, or nematic glasses, the director field $\boldsymbol{n}$ is not an independent degree of freedom. The director $\boldsymbol{n}$ is simply identical to the convected and rescaled initial director field $\boldsymbol{n}_0$

$$\boldsymbol{n} = \frac{\boldsymbol{F} \boldsymbol{n}_0}{|\boldsymbol{F} \boldsymbol{n}_0|}. \tag{17}$$

Substituting this in (13), we obtain

$$W(\boldsymbol{F}) = \frac{\mu a^{1/3}}{2} \left(\mathrm{Tr} \boldsymbol{C} - \left(\frac{a - 1}{a} \right) \frac{|\boldsymbol{C} \boldsymbol{n}_0|^2}{\boldsymbol{n}_0 \cdot \boldsymbol{C} \boldsymbol{n}_0} - \beta \boldsymbol{n}_0 \cdot \boldsymbol{C} \boldsymbol{n}_0 \right). \tag{18}$$

This can also be expressed with principal stretches by introducing the spectral representation (6).

[4] In the original work Verwey et al. (1996), the energy was described with respect to a nematic reference configuration with nematic director $\boldsymbol{n}_0$ and $\boldsymbol{l} = \boldsymbol{g}^2$ was referred to as the step-length tensor.

2.3. Membrane energy functional

With the constitutive model for bulk solids and the kinematic description of the membrane at hand we now consider the derivation of suitable membrane energy functionals. To this end we follow the work of Bhattacharya and James (1999) who derived the effective energy of thin membranes made of active materials starting from theories of bulk materials.

2.3.1. Membrane limit

In Bhattacharya and James (1999) the following energy functional is postulated for a membrane with traction free top and bottom surfaces

$$E(\boldsymbol{F}) = \int_{\Omega} \Big(c|\nabla \boldsymbol{F}|^2 + W(\boldsymbol{F}) \Big) \mathrm{d}\Omega. \tag{19}$$

The higher gradient $\nabla \boldsymbol{F} = \nabla^2 \boldsymbol{x}$ denotes the third order tensor of the second derivatives of the deformed position vector $\boldsymbol{x}$ and $c > 0$ is a scalar parameter. Higher gradient terms are common in active materials that tend to form domains, and introduce a length-scale that may be interpreted as being related to domain wall width.[5] In Bhattacharya and James (1999) it is rigorously shown that as the thickness $t \to 0$, the minimisers of the energy tend to a deformation that satisfies the property that $\boldsymbol{F}$ is uniform through the thickness (i.e., $\boldsymbol{F}$ is in independent of θ^3) and to leading order the energy of the membrane is given by the minimiser of

$$E(\boldsymbol{F}) \to t \int_{\omega} \Big(c\Big(|\nabla \bar{\boldsymbol{F}}|^2 + 2|\nabla \boldsymbol{a}_3|^2 \Big) + W\Big(\bar{\boldsymbol{F}} + \boldsymbol{a}_3 \otimes \boldsymbol{A}^3 \Big) \Big) \mathrm{d}\omega. \tag{20}$$

Here, the integral is over the membrane mid-surface ω with $\boldsymbol{x}(\theta^1, \theta^2, 0)$ and $\bar{\boldsymbol{F}}$ denotes the tangential deformation gradient defined in (7). Le Dret and Raoult (1995) studied the problem with $c = 0$ and showed that one obtains a non-convex problem due to propensity of membranes to wrinkle, and relaxing that gives rise to a tension-line theory. Shu (2000) has shown that this indeed happens even with $c > 0$ if both c and t go to zero.

In uniform isotropic materials, Dondl et al. (2007) have argued that the first two terms in the membrane energy (20) may be replaced by $\bar{c}|\mathrm{Div}\bar{\boldsymbol{F}}|^2$ for a modified coefficient $\bar{c}$. With this adaptation, the energy of the membrane may be written as

$$\bar{c}t \int_{\omega} |\mathrm{Div}\bar{\boldsymbol{F}}|^2 \mathrm{d}\omega + t \int_{\omega} W_{2D}(\bar{\boldsymbol{F}}) \mathrm{d}\omega, \tag{21}$$

where

$$W_{2D}(\bar{\boldsymbol{F}}) = \min_{\boldsymbol{a}_3} W\Big(\bar{\boldsymbol{F}} + \boldsymbol{a}_3 \otimes \boldsymbol{A}^3 \Big). \tag{22}$$

For later reference, notice that the higher order first term in (21) is the Laplacian of the mid-surface deformation, i.e. $|\mathrm{Div}\bar{\boldsymbol{F}}| = |\mathrm{Div}(\boldsymbol{a}_\alpha \otimes \boldsymbol{A}^\alpha)| = |\Delta \boldsymbol{x}(\theta^1, \theta^2, 0)|$.

In the sequel, we subject the membrane to tractions $\boldsymbol{q}$ on the boundary, and therefore write the potential energy as

$$\Pi(\bar{\boldsymbol{F}}) = \bar{c}t \int_{\omega} |\mathrm{Div}\bar{\boldsymbol{F}}|^2 \mathrm{d}\omega + t \int_{\omega} W_{2D}(\bar{\boldsymbol{F}}) \mathrm{d}\omega - \int_{\Gamma_0} \boldsymbol{q} \cdot \boldsymbol{x} \mathrm{d}\Gamma_0 := \Pi_{\mathrm{lap}} + \Pi_{\mathrm{int}} + \Pi_{\mathrm{ext}}. \tag{23}$$

2.3.2. Membrane with unconstrained nematic director

We now specialise the two-dimensional energy $W_{2D}(\bar{\boldsymbol{F}})$ (22) to the three-dimensional energy $W(\boldsymbol{F})$ of the LCE with the unconstrained nematic director (16). We assume that the membrane is subjected to extension in at least one direction while the other direction is compressed nominally. Specifically, we assume that the tangential principal stretches satisfy

$$\bar{\lambda}_1 \geqslant \bar{\lambda}_2 \geqslant \frac{1}{\bar{\lambda}_1 \bar{\lambda}_2}. \tag{24}$$

This assumption is consistent with the problems we study. The violation of this condition may lead to wrinkling instabilities that are beyond the scope of this work. We also assume that the preferred nematic director orientation is in-plane so that $\boldsymbol{A}_3 \cdot \boldsymbol{n}_0 = 0$. Under these assumptions, it is easy to show that $\bar{\boldsymbol{F}}^T \boldsymbol{a}_3 \| \boldsymbol{A}_3$ so that the nematic director remains tangential to the membrane, $\bar{\boldsymbol{E}}_\alpha$ coincides with $\boldsymbol{E}_\alpha$ and $\bar{\lambda}_\alpha = \lambda_\alpha$ for $\alpha = 1, 2$ (Cesana and Bhattacharya, 2013).[6] Physically, this means that the preferred director remains tangential to the membrane and therefore the membrane does not suffer any shear in the thickness direction. Consequently,

$$W_{2D}(\bar{\boldsymbol{F}}) = \frac{\mu a^{1/3}}{2} \left(\frac{1}{a} \bar{\lambda}_1^2 + \bar{\lambda}_2^2 + \frac{1}{(\bar{\lambda}_1 \bar{\lambda}_2)^2} - \beta \sum_{\alpha=1}^{2} \bar{\lambda}_\alpha^2 (\bar{\boldsymbol{E}}_\alpha \cdot \boldsymbol{n}_0)^2 \right). \tag{25}$$

2.3.3. Membrane with frozen nematic director

We similarly specialise the two-dimensional energy $W_{2D}(\bar{\boldsymbol{F}})$ (22) to the three-dimensional energy $W(\boldsymbol{F})$ of the LCE with the frozen nematic director (18). As before if we assume that $\boldsymbol{n}_0$ is in-plane so that $\boldsymbol{A}_3 \cdot \boldsymbol{n}_0 = 0$, and that the principal values of the tangential deformation gradient satisfies (24). We can conclude as before that for the minimising $\boldsymbol{a}_3$, two of the principal values and directions of $\boldsymbol{F}$ coincide with those of $\bar{\boldsymbol{F}}$. Therefore, we obtain

$$W_{2D}(\bar{\boldsymbol{F}}) = \frac{\mu a^{1/3}}{2} \left(\mathrm{Tr}\,\bar{\boldsymbol{C}} + \frac{1}{\det \bar{\boldsymbol{C}}} - \left(\frac{a-1}{a} \right) \frac{|\bar{\boldsymbol{C}}\boldsymbol{n}_0|^2}{\boldsymbol{n}_0 \cdot \bar{\boldsymbol{C}}\boldsymbol{n}_0} - \beta \boldsymbol{n}_0 \cdot \bar{\boldsymbol{C}}\boldsymbol{n}_0 \right). \tag{26}$$

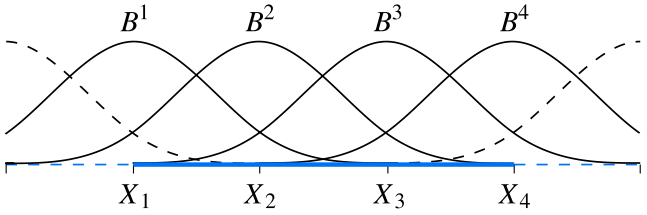

Fig. 4. One dimensional domain with four nodes $\boldsymbol{X}_1, \boldsymbol{X}_2, \boldsymbol{X}_3$ and $\boldsymbol{X}_4$ and the corresponding qubic b-spline basis functions. In the elements on the domain boundaries, i.e. elements $[\boldsymbol{X}_1, \boldsymbol{X}_2]$ and $[\boldsymbol{X}_3, \boldsymbol{X}_4]$, the interpolation is incomplete and the computational domain has to be chosen slightly larger than the physical domain. The dashed elements and b-splines are the so-called guard or ghost elements.

3. Finite element discretization

We discretize the energy functional of the nematic membrane (23) with finite elements. As basis functions we use quartic box-splines, which yield C^2 continuous surfaces and have finite square integrable first and second order derivatives. Smooth basis functions are necessary because of the second order derivatives included in the Laplacian regularisation term $|\mathrm{Div}\bar{\boldsymbol{F}}|$.

Without going into details, we assume that the membrane surface is meshed with triangular elements and that the reference and deformed membrane surfaces can be approximated with

[5] In liquid crystal elastomers, domain wall width is governed by Frank elasticity (Warner and Terentjev, 2007) that depends on the gradient of the director. So the term here is not strictly correct, but instead serves as a surrogate giving rise to similar physics.

[6] This result valid even if we relax (24) except in non-generic cases, but is easily proved under (24).

$$\boldsymbol{X} \approx \boldsymbol{X}^h = \sum_i^N B^i(\theta^1, \theta^2)\boldsymbol{X}_i, \qquad \boldsymbol{x} \approx \boldsymbol{x}^h = \sum_i^N B^i(\theta^1, \theta^2)\boldsymbol{x}_i, \tag{27}$$

where $B^i(\theta^1, \theta^2)$ are the box-spline basis functions belonging to node i, and $\boldsymbol{X}_i$ and $\boldsymbol{x}_i$ are the corresponding nodal coordinates in the reference and deformed configurations, respectively. The total number of the nodes of the mesh is N. As an example, Fig. 4 shows the one-dimensional b-spline basis functions over a one-dimensional domain with four nodes. The depicted cubic b-splines are equivalent to the quartic box-splines used in the two-dimensional setting with triangular elements. We refer to Cirak et al. (2000), Cirak and Ortiz (2001) and Cirak and Long (2011) for a detailed discussion on basis functions.

The discretised energy functional for the nematic membrane is obtained by introducing interpolation Eqs. (27) into the energy functional (23) and subsequent element-by-element numerical integration in a finite element sense. In order to compute the kinematic expressions appearing in the energy functional, such as the covariant and contravariant base vectors introduced in Section 2.1, notice that the basis functions $B^i(\theta^1, \theta^2)$ are defined over the parameter space with the coordinates (θ^1, θ^2). The discrete equilibrium equations follow from the stationarity condition for the discretized energy functional

$$\frac{\partial \Pi(\boldsymbol{x}^h)}{\partial \boldsymbol{x}^h} = \underbrace{\frac{\partial \Pi_{\text{lap}}(\Delta \boldsymbol{x}^h)}{\partial \boldsymbol{x}^h} + \frac{\partial \Pi_{\text{int}}(\boldsymbol{C}(\boldsymbol{x}^h))}{\partial \boldsymbol{C}} \frac{\partial \boldsymbol{C}}{\partial \boldsymbol{x}^h}}_{\boldsymbol{f}^h_{\text{int}}} + \underbrace{\frac{\partial \Pi_{\text{ext}}(\boldsymbol{x}^h)}{\partial \boldsymbol{x}^h}}_{-\boldsymbol{f}^h_{\text{ext}}} = \boldsymbol{0}, \tag{28}$$

where $\boldsymbol{f}^h_{\text{int}}$ is the internal force vector and $\boldsymbol{f}^h_{\text{ext}}$ is the external force vector. For more details on computing (28) for the considered membrane energies see A and B.

The solution of the discrete non-linear equations

$$\boldsymbol{f}^h_{\text{int}}(\boldsymbol{x}^h) - \boldsymbol{f}^h_{\text{ext}} = \boldsymbol{0}, \tag{29}$$

is the equilibrium configuration of the membrane. Even in case of convex constitutive models, these discrete equilibrium equations can have several solutions, for instance, in case of buckling of compressed membranes. The non-uniqueness of the discrete equilibrium equations usually manifests itself in non-convergent solution algorithms. To sidestep the problem of non-uniqueness in the numerical solution stage we consider a dynamic relaxation method (Oakley and Knight, 1995; Cirak and Ortiz, 2001). This means, the steady-state solution is obtained as the long term solution of a damped dynamic system

$$\boldsymbol{m}\ddot{\boldsymbol{x}}^h + \boldsymbol{c}\dot{\boldsymbol{x}}^h + \boldsymbol{f}^h_{\text{int}}(\boldsymbol{x}^h) - \boldsymbol{f}^h_{\text{ext}} = \boldsymbol{0}, \tag{30}$$

where $\boldsymbol{m}$ is the mass matrix and $\boldsymbol{c}$ is a damping matrix. For a membrane with areal density ρ the mass matrix is defined with

$$\boldsymbol{m} = \rho \int_{\omega_0} B^i B^j \, d\omega_0. \tag{31}$$

We choose the damping matrix of the same form as the mass matrix

$$\boldsymbol{c} = \eta \int_{\omega_0} B^i B^j \, d\omega_0, \tag{32}$$

where η is a scalar damping parameter. In the numerical computations, the parameters ρ and η are chosen such that the semidiscrete equilibrium Eqs. (30) represent a critically damped system. We integrate the semidiscrete equilibrium equations with the explicit Newmark scheme, see e.g. Hughes (1987).

4. Energetics of deformations from flat to non-developable surfaces

We numerically study the soft behaviour of a rectangular nematic membrane with the introduced model. The membrane is flat in its reference configuration, see Fig. 5. The nematic director initially points along $\boldsymbol{X}_2$ direction, i.e. $\boldsymbol{n}_0 = (0 \quad 1)^{\mathsf{T}}$. The membrane is deformed into two different configurations by applying prescribed displacements to the membrane boundaries. In the first case, the membrane is deformed into a developable surface in the form of part of a cylinder, see Fig. 6. In the second case, the membrane is forced into a non-developable saddle shape by prescribing at the left boundary a circular arc pointing downwards and at the right boundary an arc pointing upwards, see Fig. 7. In both cases the parameter κ is chosen such that the opening angle of the arc is 80° and its length is equal to the side length l_2 of the rectangle. Depending on the form of prescribed boundary position, the two cases are referred to in the following as Up–Up and Down–Up.

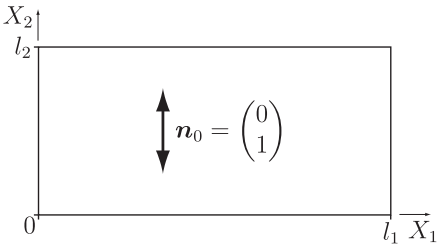

Fig. 5. Geometry of the membrane in the reference configuration and the nematic director vector.

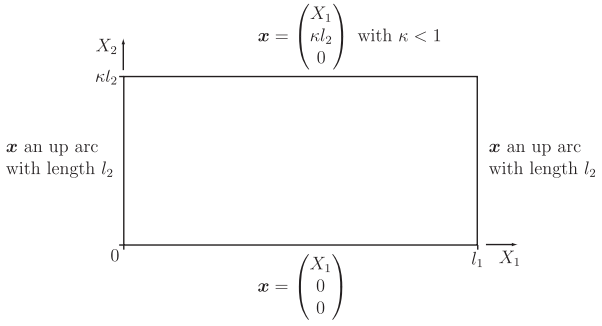

Fig. 6. Prescribed boundaries in the deformed configuration (Up–Up).

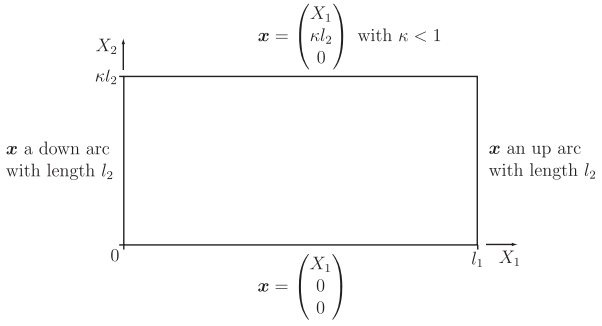

Fig. 7. Prescribed boundaries in the deformed configuration (Down–Up).

4.1. Parameters

We take the rectangular nematic membrane to be $l_1 = 10$ mm $\times$ $l_2 = 4$ mm in lateral extent and $t = 0.1$ mm in thickness in the reference configuration. We take the parameter a in the step-length tensor $\boldsymbol{g}$ to be 2.0, c.f. (10), and the non-ideality parameter to be $\beta = 0.05$, c.f. (13), consistent with these materials Warner and

Terentjev (2007). We take the membrane shear modulus $\mu t = 7.937$ N/m consistent with our chosen thickness and typical shear moduli of liquid crystal elastomers ($\approx 10^5$ N/m^2) (Warner and Terentjev, 2007). For the chosen energy (21), we expect the width of the domain wall to be of the order of $\sqrt{c/\mu}$. This is often termed as the nematic penetration depth, and has been estimated to be of the order of 10 nm. A slightly larger value may be appropriate in our setting since a membrane has some bending stiffness and this will add a contribution to the first term in the energy. Further, a small value poses a problem in computations since the numerical discretization has to be smaller than this length and the computation extent has to be of the size of the specimen. Therefore, we choose this length to be large, $\sqrt{c/\mu} = 0.2806$ mm. We note that this turns out to be conservative in our setting – choosing a smaller value for this parameter would only make our conclusions stronger. We discretize our computational domain with 64561 nodes and 128000 triangular elements of size $h = 0.025$ mm. This ensures that we resolve the domain walls, if any, fully while the domain is large enough for microstructures to develop. In other words, our choice of parameters satisfy $h \ll \sqrt{c/\mu} \ll l_1$ which is necessary for such computations.

4.2. Membrane with frozen nematic director

In the first set of computations we consider a membrane made of a LCE with a frozen nematic director described in Section 2.3.3. The deformed configurations of the two cases with different prescribed boundary conditions are shown in Fig. 8. The corresponding contour plots of the out-of-plane displacements are depicted in Fig. 9. In the Up–Up case the membrane deforms into an almost cylindrical shape. It is not an exact cylinder because of the incompressibility of the material and the resulting coupling of the deformations in the longitudinal and circumferential directions. In the Down–Up case the membrane deforms into a saddle-like shape which requires substantial straining of the membrane in its longitudinal midsection. In the computations the specific location of the

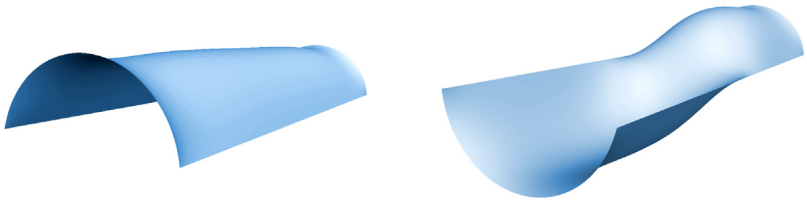

(a) Up-Up (b) Down-Up

Fig. 8. Deformed configurations of the LCE membrane with frozen director.

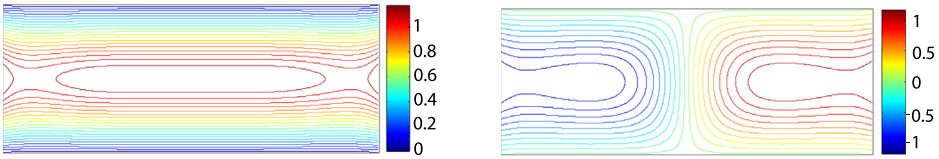

(a) Up-Up (b) Down-Up

Fig. 9. Out-of-plane displacement isolines of the LCE membranes with frozen director.

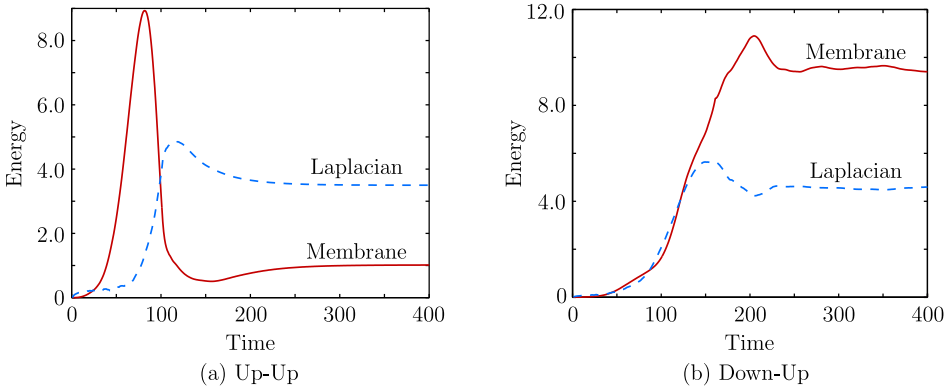

(a) Up-Up (b) Down-Up

Fig. 10. Convergence histories of the membrane and Laplacian energies of the LCE membranes with frozen director. All energies in $\times 10^{-6}$ Nm.

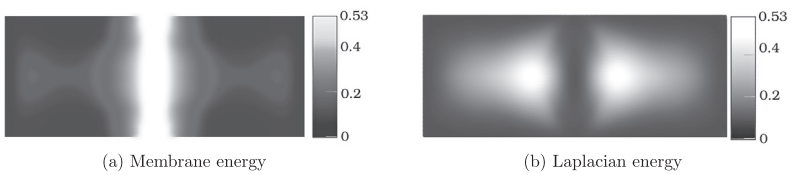

(a) Membrane energy (b) Laplacian energy

Fig. 11. Energy contours of the LCE membrane with the frozen director in the Down–Up case.

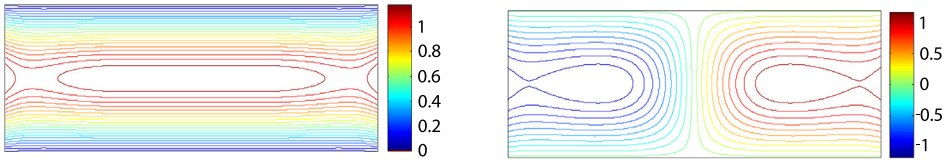

(a) Up-Up (b) Down-Up

Fig. 12. Out-of-plane displacement isolines of the LCE membrane with unconstrained director.

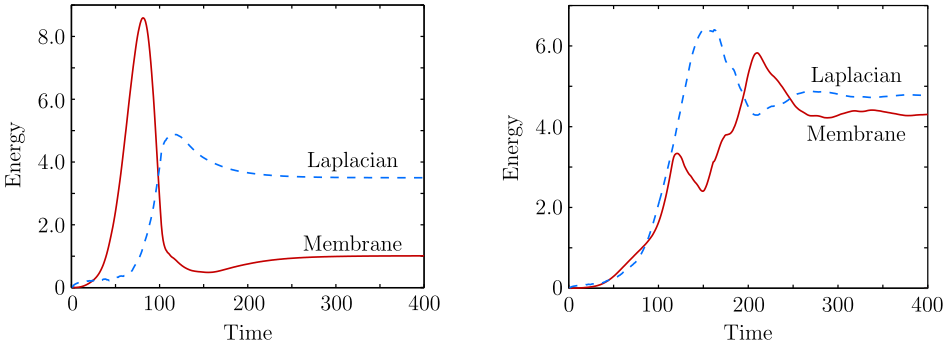

(a) Up-Up (b) Down-Up

Fig. 13. Convergence histories of the membrane and Laplacian energies of the LCE membranes with unconstrained director. All energies in $\times 10^{-6}$ Nm.

transition from down deformation into up deformation is enforced by initial imperfections in form of pressure loading. This pressure loading is applied during the initial phase of the computations and is later removed.

In Fig. 10 the iteration histories for the two cases are plotted. As introduced in Section 3, we use a dynamic relaxation technique for computing the equilibrium configurations in which each iteration step corresponds to a pseudo time-step. During the iterations the membrane as well as the Laplacian energies are monitored. It can be assumed that an equilibrium configuration is obtained when both energies converge. It can be seen in Fig. 10 that the converged membrane energy in the Up–Up case is 1.01×10^{-6} Nm and in the Down–Up case 9.41×10^{-6} Nm. The reason for the larger membrane energy in the Down–Up case is the non-developable shape of the deformed configuration. The Laplacian energy in the Up–Up case is 3.50×10^{-6} Nm and in the Down–Up case is 4.59×10^{-6} Nm.

The energy contours of the Down–Up case provide a more detailed insight into the partition of the total energy into membrane and Laplacian components, see Fig. 11. The membrane energy is localised around the longitudinal middle of the membrane where it is forced to remain flat and is subjected to vertical compressive strain. In contrast, due to the flatness of the middle section the Laplacian energy is negligible. The Laplacian energy is localised around the regions with non-zero curvature.

4.3. Membrane with unconstrained nematic director

In the second set of computations we consider a membrane made of a LCE with an unconstrained nematic director. During the deformations the nematic director is allowed to reorient in order to minimise the total energy. The internal energy density is as given in (25).

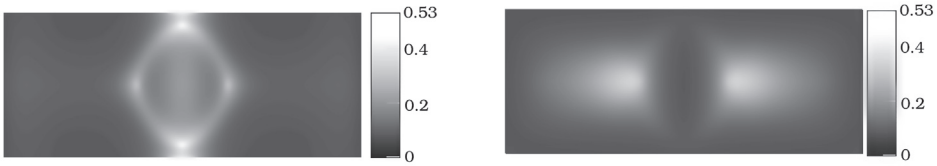

(a) Membrane energy (b) Laplacian energy

Fig. 14. Energy contours of the LCE membrane with unconstrained director in the Down–Up case.

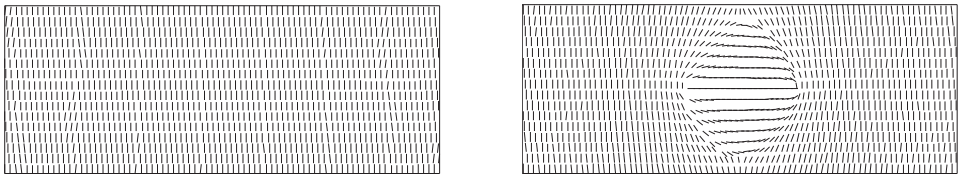

(a) Up-Up (b) Down-Up

Fig. 15. Nematic director fields of the deformed LCE membrane.

In Fig. 12 the out-of-plane displacement isolines for the Up–Up and Down–Up cases are plotted, which are visually indistinguishable from the corresponding plots for the LCE with frozen director in Fig. 9. Despite the displacements being almost identical, the internal energies are not the same as in the constrained director case, see Fig. 13. This is particularly apparent in the Down–Up case where the membrane energy is 4.30×10^{-6} Nm and the Laplacian energy is 4.76×10^{-6} Nm. This means that the Laplacian energies in the unconstrained and constrained director cases are almost identical. However, the membrane energy in the unconstrained case is by a factor ≈ 2.2 smaller than in the constrained case. As can be seen in Fig. 14, this reduction in energy occurs primarily in the longitudinal middle section of the membrane. The energies in the LCE membranes with constrained and unconstrained director are very different despite the macroscopically observed strain in both is very similar (since the displacements are very similar).

The relative softness of the LCE membrane with the unconstrained nematic director can be explained with the rotation of the director. Pointwise the director can rotate in a configuration which minimises the membrane energy density. As can be seen in Fig. 15(b), in the diamond shaped midsection of the membrane the initial director $\boldsymbol{n}_0 = (0 \quad 1)^{\mathsf{T}}$ becomes after rotation $\boldsymbol{n} = (1 \quad 0)^{\mathsf{T}}$. This rotation reduces pointwise the amount of straining in the vertical direction according to (10). Note that in the presented formulation the rapid oscillation of the director field is prohibited by the Laplacian energy included. Hence the material is not allowed to form laminates as reported, e.g., in Conti et al. (2002). In Fig. 15(a) the nematic director field in the Up–Up case is depicted. Because the deformed cylindrical surface is developable and the membrane strains are small, the nematic director does not reorient itself.

5. Conclusions

We have presented a computational technique for determining the equilibrium shapes of LCE membranes. The membrane deformations can be finite and the initial shape of the membrane does not need to be flat. The included Laplacian energy prohibits the rapid oscillations of the nematic director on a scale smaller than the spatial resolution of the used finite element mesh. Hence, physically meaningful results are obtained even in the presence of non-convex energy functionals. The proposed membrane energy functional is discretized with finite elements using structured triangular meshes and box-splines. In case of complex domains with arbitrary connectivity meshes subdivision finite elements can be used (Cirak et al., 2000; Cirak and Ortiz, 2001; Cirak and Long, 2011; Long et al., 2012).

From an application viewpoint, we numerically demonstrated that it is possible to obtain from flat sheets surfaces with non-zero Gaussian curvature with minimal stretch energy. The necessary change of the surface metric in the transition from flat to non-zero Gaussian curvature is accomplished by the reorientation of the nematic director. This can be exploited in designing highly efficient microscale actuators. It is possible to first deform a flat membrane into a shape with non-zero Gaussian curvature using only minimum amount of energy. Subsequently, the director orientations can be selectively reoriented to their reference configuration using, for example, illumination or heat. The accompanying sudden deformation of the membrane towards the reference configuration can be used for performing external work. Here, it is important that the membrane energy scales linearly with the thickness t and the bending energy scales with t^3. Hence, the mechanical work that can be extracted with devices operating in a membrane mode, such as the considered LCE membranes, is larger than with conventional devices operating in a bending mode.

Appendix A. Derivation of stresses

The stresses corresponding to the liquid crystalline elastomer models are obtained by differentiating the introduced energy densities. First, we consider the unconstrained nematic director with the energy density (25). Differentiating it with respect to the right Cauchy–Green strain tensor yields the second Piola–Kirchhoff stress tensor

$$\boldsymbol{S} = 2\frac{\partial W_{2D}}{\partial \bar{\boldsymbol{C}}} = 2\frac{\partial W_{2D}}{\partial \bar{\lambda}_\alpha^2}\frac{\partial \bar{\lambda}_\alpha^2}{\partial \bar{\boldsymbol{C}}}$$

with

$$\frac{\partial W_{2D}}{\partial \bar{\lambda}_1^2} = \frac{\mu a^{1/3}}{2}\left(\frac{1}{a} - \frac{1}{\bar{\lambda}_1^4\bar{\lambda}_2^2} - \beta(\bar{\boldsymbol{E}}_1 \cdot \boldsymbol{n}_0)^2\right) \tag{A.1a}$$

$$\frac{\partial W_{2D}}{\partial \bar{\lambda}_2^2} = \frac{\mu a^{1/3}}{2}\left(1 - \frac{1}{\bar{\lambda}_1^2\bar{\lambda}_2^4} - \beta(\bar{\boldsymbol{E}}_2 \cdot \boldsymbol{n}_0)^2\right). \tag{A.1b}$$

For the derivatives of the stretches with respect to the right Cauchy–Green strain tensor the following relation is known

$$\frac{\partial \bar{\lambda}_\alpha^2}{\partial \bar{\boldsymbol{C}}} = \bar{\boldsymbol{E}}_\alpha \otimes \bar{\boldsymbol{E}}_\alpha$$

which is clear from $\bar{\lambda}_\alpha^2 = \bar{\boldsymbol{C}} : \bar{\boldsymbol{E}}_\alpha \otimes \bar{\boldsymbol{E}}_\alpha$.

Next, we consider the frozen nematic director with the energy density (26). The derivatives of this energy density with respect to the eigenvalues of $\bar{\boldsymbol{C}}$ are

$$\frac{\partial W_{2D}}{\partial \bar{\lambda}_1^2} = \frac{\mu a^{1/3}}{2}\left(1 - \frac{1}{\bar{\lambda}_1^4\bar{\lambda}_2^2} - \alpha\frac{\partial|\bar{\boldsymbol{C}}\boldsymbol{n}_0|^2}{\partial \bar{\lambda}_1^2}\frac{1}{\boldsymbol{n}_0 \cdot \bar{\boldsymbol{C}}\boldsymbol{n}_0} + \left(\alpha\frac{|\bar{\boldsymbol{C}}\boldsymbol{n}_0|^2}{(\boldsymbol{n}_0 \cdot \bar{\boldsymbol{C}}\boldsymbol{n}_0)^2} - \beta\right)(\bar{\boldsymbol{E}}_1 \cdot \boldsymbol{n}_0)^2\right) \tag{A.2a}$$

$$\frac{\partial W_{2D}}{\partial \lambda_2^2} = \frac{\mu a^{1/3}}{2}\left(1 - \frac{1}{\bar{\lambda}_1^2\bar{\lambda}_2^4} - \alpha\frac{\partial|\bar{\boldsymbol{C}}\boldsymbol{n}_0|^2}{\partial \lambda_2^2}\frac{1}{\boldsymbol{n}_0 \cdot \bar{\boldsymbol{C}}\boldsymbol{n}_0} + \left(\alpha\frac{|\bar{\boldsymbol{C}}\boldsymbol{n}_0|^2}{(\boldsymbol{n}_0 \cdot \bar{\boldsymbol{C}}\boldsymbol{n}_0)^2} - \beta\right)(\bar{\boldsymbol{E}}_2 \cdot \boldsymbol{n}_0)^2\right) \tag{A.2b}$$

with $\alpha = 1 - a^{-1}$ and the derivatives

$$\frac{\partial|\bar{\boldsymbol{C}}\boldsymbol{n}_0|^2}{\partial \bar{\lambda}_1^2} = 2\bar{\lambda}_1^2(\bar{\boldsymbol{E}}_1 \cdot \boldsymbol{n}_0)^2, \qquad \frac{\partial|\bar{\boldsymbol{C}}\boldsymbol{n}_0|^2}{\partial \bar{\lambda}_2^2} = 2\bar{\lambda}_2^2(\bar{\boldsymbol{E}}_2 \cdot \boldsymbol{n}_0)^2,$$

which follow directly from differentiating

$$|\bar{\boldsymbol{C}}\boldsymbol{n}_0|^2 = \boldsymbol{n}_0 \cdot \left(\sum_{I=1}^{2}\bar{\lambda}_I^4(\bar{\boldsymbol{E}}_I \otimes \bar{\boldsymbol{E}}_I)\right)\boldsymbol{n}_0.$$

Appendix B. Second gradient of the deformation

As introduced in Section 2.3.1 the second gradient of the deformation are considered for regularisation purposes. The Laplacian of the deformation is defined as,

$$\Delta\boldsymbol{x}(\theta^1, \theta^2, 0) = \mathrm{Div}\,\bar{\boldsymbol{F}} = \mathrm{Div}\,(\boldsymbol{a}_\alpha \otimes \boldsymbol{A}^\alpha) \tag{B.1}$$

which reads in index notation

$$\Delta\boldsymbol{x}(\theta^1, \theta^2, 0) = \frac{\partial}{\partial X_j}\left(\frac{\partial x_i}{\partial \theta^\alpha}\frac{\partial \theta^\alpha}{\partial X_j}\right) = \frac{\partial^2 x_i}{\partial \theta^\alpha \partial \theta^\gamma}\frac{\partial \theta^\gamma}{\partial X_j}\frac{\partial \theta^\alpha}{\partial X_j} + \frac{\partial x_i}{\partial \theta^\alpha}\frac{\partial^2 \theta^\alpha}{\partial X_j^2}. \tag{B.2}$$

To evaluate this expression recall the following standard relations from differential geometry

$$\boldsymbol{A}^\alpha = A^{\alpha\beta}\boldsymbol{A}_\beta, \tag{B.3a}$$

$$\boldsymbol{A}_\alpha = A_{\alpha\beta}\boldsymbol{A}^\beta, \tag{B.3b}$$

$$A^{\alpha\beta}A_{\beta\gamma} = \delta^{\alpha}_{\gamma}, \tag{B.3c}$$

where $A_{\alpha\beta} = \boldsymbol{A}_\alpha \cdot \boldsymbol{A}_\beta$ is the covariant metric tensor in the reference configuration. The Eqs. (B.3a) and (B.3b) read in index notation

$$\frac{\partial \theta^\alpha}{\partial X_j} = \left(\frac{\partial \theta^\alpha}{\partial X_i}\frac{\partial \theta^\beta}{\partial X_i}\right)\frac{\partial X_j}{\partial \theta^\beta}, \qquad \frac{\partial X_j}{\partial \theta^\alpha} = \left(\frac{\partial X_i}{\partial \theta^\alpha}\frac{\partial X_i}{\partial \theta^\beta}\right)\frac{\partial \theta^\beta}{\partial X_j}. \tag{B.4}$$

To compute the last derivative appearing in (B.2) we consider

$$\begin{aligned}\frac{\partial^2 \theta^\alpha}{\partial X_j^2} &= \frac{\partial}{\partial X_j}\left[\left(\frac{\partial \theta^\alpha}{\partial X_i}\frac{\partial \theta^\beta}{\partial X_i}\right)\frac{\partial X_j}{\partial \theta^\beta}\right] = \frac{\partial}{\partial X_j}\left[\left(\frac{\partial X_i}{\partial \theta^\alpha}\frac{\partial X_i}{\partial \theta^\beta}\right)^{-1}\frac{\partial X_j}{\partial \theta^\beta}\right] \\ &= \frac{\partial}{\partial X_j}\left(\frac{\partial X_i}{\partial \theta^\alpha}\frac{\partial X_i}{\partial \theta^\beta}\right)^{-1}\frac{\partial X_j}{\partial \theta^\beta} + \left(\frac{\partial X_i}{\partial \theta^\alpha}\frac{\partial X_i}{\partial \theta^\beta}\right)^{-1}\frac{\partial}{\partial X_j}\frac{\partial X_j}{\partial \theta^\beta}\end{aligned} \tag{B.5}$$

wherein the derivative of the inverse of the covariant metric tensor $A_{\alpha\beta}$ can be obtained by differentiating (B.3c), i.e.

$$\frac{\partial}{\partial X_j}\left(A^{\alpha\beta}A_{\beta\gamma}\right) = 0. \tag{B.6}$$

References

Bhattacharya, K., James, R.D., 1999. A theory of thin films of martensitic materials with applications to microactuators. Journal of the Mechanics and Physics of Solids 47 (3), 531–576.

Bhattacharya, K., Li, J., Xiao, Y., 2001. Electromechanical models for optimal design and effective behavior of electroactive polymers. SPIE Press.

Biggins, J.S., Terentjev, E.M., Warner, M., 2008. Semisoft elastic response of nematic elastomers to complex deformations. Phys. Rev. E 78, 041704.

Cesana, P., Bhattacharya, K., (2013). Effective energy of nematic elastomer membranes. In preparation.

Cirak, F., Long, Q., 2011. Subdivision shells with exact boundary control and non-manifold geometry. International Journal for Numerical Methods in Engineering 88, 897–923.

Cirak, F., Ortiz, M., 2001. Fully C^1-conforming subdivision elements for finite deformation thin-shell analysis. International Journal for Numerical Methods in Engineering 51, 813–833.

Cirak, F., Ortiz, M., Schröder, P., 2000. Subdivision surfaces: a new paradigm for thin-shell finite-element analysis. International Journal for Numerical Methods in Engineering 47, 2039–2072.

Cirak, F., Cisternas, J.E., Cuitino, A.M., Ertl, G., Holmes, P., Kevrekidis, I.G., Ortiz, M., Rotermund, H.H., Schunack, M., Wolff, J., 2003. Oscillatory thermomechanical instability of an ultrathin catalyst. Science 300, 1932–1936.

Conti, S., DeSimone, A., Dolzmann, G., 2002. Soft elastic response of stretched sheets of nematic elastomers: a numerical study. Journal of the Mechanics and Physics of Solids 50, 1431–1451.

Corbett, D., Warner, M., 2009. Electromechanical elongation of nematic elastomers for actuation. Sensors and Actuators A: Physical 149, 120–129.

DeSimone, A., Dolzmann, G., 2002. Macroscopic response of nematic elastomers via relaxation of a class of SO(3)-invariant energies. Archive for Rational Mechanics and Analysis 161, 181–204.

DeSimone, A., Teresi, L., 2009. Elastic energies for nematic elastomers. The European Physical Journal E 29, 191–204.

Dondl, P.W., Shen, C.-P., Bhattacharya, K., 2007. Computational analysis of martensitic thin films using subdivision surfaces. International Journal for Numerical Methods in Engineering 72, 72–94.

Finkelmann, H., Kundler, I., Terentjev, E.M., Warner, M., 1997. Critical stripe-domain instability of nematic elastomers. Journal de Physics II France 7, 1059–1069.

Gurtin, M.E., Fried, E., Anand, L., 2010. The Mechanics and Thermodynamics of Continua. Cambridge University Press.

Hughes, T.J.R., 1987. The finite element method: linear static and dynamic finite element analysis. Prentice-Hall Inc..

Kohn, R.V., Müller, S., 1992. Relaxation and regularization of nonconvex variational problems. Rendiconti del Seminario Matematico e Fisico di Milano 62, 89–113.

Le Dret, H., Raoult, A., 1995. The nonlinear membrane model as variational limit of nonlinear three-dimensional elasticity. Journal de Mathématiques Pures et Appliquées 74, 549–578.

Long, Q., Bornemann, P.B., Cirak, F., 2012. Shear-flexible subdivision shells. International Journal for Numerical Methods in Engineering 90, 1549–1577.

Modes, C.D., Bhattacharya, K., Warner, M., 2011. Gaussian curvature from flat elastica sheets. Proceedings of the Royal Society A: Mathematical, Physical and Engineering Sciences 467, 1121–1140.

Mosler, J., Cirak, F., 2009. A variational formulation for finite deformation wrinkling analysis of inelastic membranes. Computer Methods in Applied Mechanics and Engineering 198, 2087–2098.

Oakley, D.R., Knight Jr., N.F., 1995. Adaptive Dynamic Relaxation algorithm for non-linear hyperelastic structures. Part I. Formulation. Computer Methods in Applied Mechanics and Engineering 126, 67–89.

Pipkin, A.C., 1994. Relaxed energy densities for large deformations of membranes. IMA Journal of Applied Mathematics 52, 297–308.

Shu, Y.C., 2000. Heterogeneous thin films of martensitic materials. Archive for Rational Mechanics and Analysis 153 (1), 39–90.

van Oosten, C.L., Corbett, D., Davies, D., Warner, M., Bastiaansen, C.W.M., Broer, D.J., 2008. Bending dynamics and directionality reversal in liquid crystal network photoactuators. Macromolecules 41, 8592–8596.

van Oosten, C.L., Bastiaansen, C.W.M., Broer, D.J., 2009. Printed artificial cilia from liquid-crystal network actuators modularly driven by light. Nature Materials 8, 677–682.

Verwey, G.C., Warner, M., Terentjev, E.M., 1996. Elastic instability and stripe domains in liquid crystalline elastomers. Journal de Physique 6, 1273–1290.

Warner, M., Mahadevan, L., 2004. Photoinduced deformations of beams, plates, and films. Physical Review Letters 92.

Warner, M., Terentjev, E.M., 2007. Liquid crystal elastomers, . International Series of Monographs of Physics, second paperback ed. Oxford University Press.

Warner, M., Modes, C.D., Corbett, D., 2010a. Curvature in nematic elastica responding to light and heat. Proceedings of the Royal Society A: Mathematical, Physical and Engineering Sciences 466, 2975–2989.

Warner, M., Modes, C.D., Corbett, D., 2010b. Suppression of curvature in nematic elastica. Proceedings of the Royal Society A: Mathematical, Physical and Engineering Sciences 466, 3561–3578.